nature geoscience

ARTICLES

PUBLISHED ONLINE: 10 NOVEMBER 2013 | DOI: 10.1038/NGEO1999

Statistically derived contributions of diverse human influences to twentieth-century temperature changes

Francisco Estrada[1,2]*, Pierre Perron[3] and Benjamín Martínez-López[1]

The warming of the climate system is unequivocal as evidenced by an increase in global temperatures by 0.8 °C over the past century. However, the attribution of the observed warming to human activities remains less clear, particularly because of the apparent slow-down in warming since the late 1990s. Here we analyse radiative forcing and temperature time series with state-of-the-art statistical methods to address this question without climate model simulations. We show that long-term trends in total radiative forcing and temperatures have largely been determined by atmospheric greenhouse gas concentrations, and modulated by other radiative factors. We identify a pronounced increase in the growth rates of both temperatures and radiative forcing around 1960, which marks the onset of sustained global warming. Our analyses also reveal a contribution of human interventions to two periods when global warming slowed down. Our statistical analysis suggests that the reduction in the emissions of ozone-depleting substances under the Montreal Protocol, as well as a reduction in methane emissions, contributed to the lower rate of warming since the 1990s. Furthermore, we identify a contribution from the two world wars and the Great Depression to the documented cooling in the mid-twentieth century, through lower carbon dioxide emissions. We conclude that reductions in greenhouse gas emissions are effective in slowing the rate of warming in the short term.

Two main statistical approaches are used to investigate the attribution of climate change: the optimal fingerprinting method[1], which consists of searching for spatial and/or temporal patterns consistent with the anthropogenic forcing signals that are common to observed and externally forced simulations of climate variables, and the cointegration framework that permits testing for the attribution of climate change directly from observed temperature and radiative forcing data[2]. As shown, temperature and radiative forcings are not integrated processes once breaks in trend are accounted for, rendering the latter approach inappropriate[3,4]. We therefore use recently developed statistical methods to analyse the properties of trending series[5–9]. We focus on providing evidence for the existence of a nonlinear trend characterized by breaks in slope that are common to observed global and hemispheric temperatures and anthropogenic forcing, thereby establishing direct evidence for the effect of human factors in altering the long-run path of global and hemispheric temperatures. Once this nonlinear trend is accounted for, all remaining variations in temperatures are stationary with different durations explained mostly by non-human factors. Our results are robust to different choices for temperatures and mixtures of anthropogenic and natural forcing series.

Analysis of the observed warming trends in temperatures

The data for global, Southern Hemisphere and Northern Hemisphere temperatures are from the National Aeronautics and Space Administration (NASA) database and the Climatic Research Unit HadCRUT4 (see Fig. 1). Results for the HadCRUT3 data set are also presented in the Supplementary Information. The forcing variables are the radiate forcing of greenhouse gases (RFGHG) mainly produced by anthropogenic activities, the sum of all radiative forcing variables except the two main natural sources, solar and stratospheric aerosols (TRF*) as explained in the Methods, and TRF which is the sum of TRF* plus solar forcing and represents a mixture of all natural and anthropogenic radiative forcing variables that are trending.

The Atlantic Multidecadal Oscillation (AMO) represents ocean–atmosphere processes naturally occurring in the North Atlantic with a large influence over Northern Hemisphere and global climates[10,11]. It produces 60- to 90-year natural oscillations that distort the warming trend suggesting it should be filtered before conducting attribution studies[10,12]. After detrending global and Northern Hemisphere with TRF, the residuals are highly correlated with AMO, indicating the importance of this mode of variability for explaining the low-frequency variability in global and Northern Hemisphere (Supplementary Information 1). Consequently, we remove the low-frequency natural component of the AMO to obtain a better measure of the low-frequency trend, that is, to isolate the trend in climate. The filtered global and Northern Hemisphere and unfiltered Southern Hemisphere temperature series are graphed in Fig. 1. A visual inspection clearly suggests nonlinear trend functions with an abrupt change in the warming rates[3,13].

To statistically document the presence of a break in the trend of temperature series, we use the Perron–Yabu[7] testing procedure, valid with integrated or stationary noise, circumventing the problem of pretesting for unit roots. The null hypothesis of no-break is rejected in all cases at the 1% significance level. Consider the regression

$$y_t = \mu + \beta_1 t + \beta_2 DT_t^* + \tilde{y}_t \quad (1)$$

[1]Centro de Ciencias de la Atmósfera, Universidad Nacional Autónoma de México, Ciudad Universitaria, Circuito Exterior, 04510 Mexico, DF, Mexico, [2]Institute for Environmental Studies, Vrije Universiteit, Amsterdam, Netherlands, [3]Department of Economics, Boston University, 270 Bay State Rd. Boston, Massachusetts 02215, USA. *e-mail: feporrua@atmosfera.unam.mx

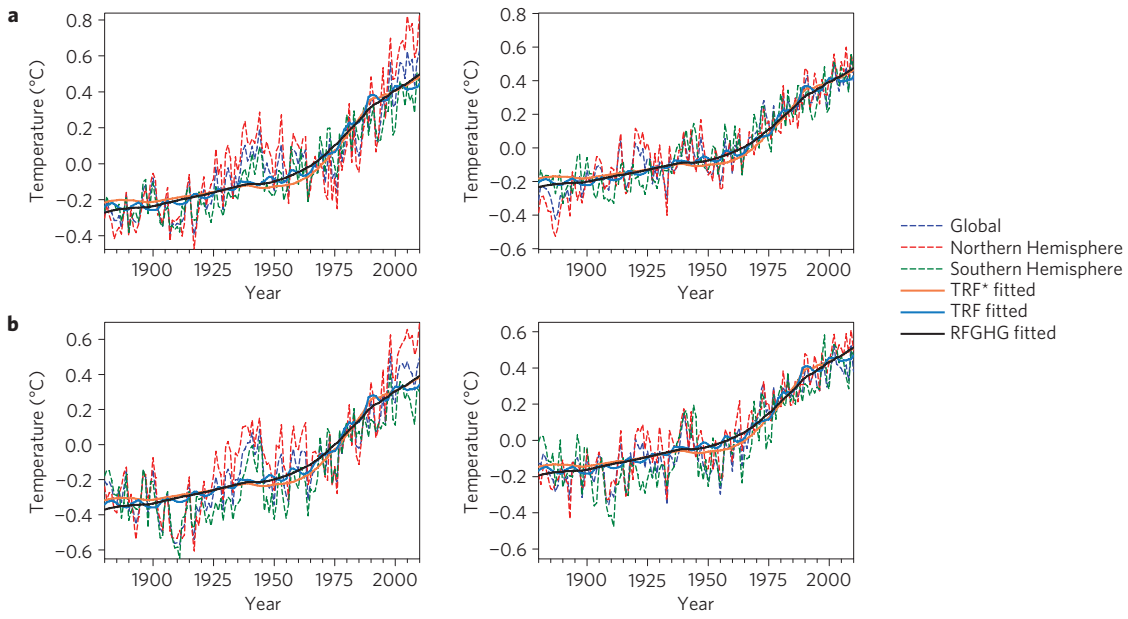

Figure 1 | Filtered and unfiltered temperature series. a, Dashed lines show the observed global, Northern Hemisphere and Southern Hemisphere (left panel) and the filtered global and Northern Hemisphere and unfiltered Southern Hemisphere (right panel) for the NASA data set. The solid lines represent the fitted temperature series using RFGHG, TRF* and TRF. **b**, Dashed lines show the observed global, Northern Hemisphere and Southern Hemisphere (left panel) and the filtered global and Northern Hemisphere and unfiltered Southern Hemisphere (right panel) for the HadCRUT4 data set. The solid lines represent the fitted temperature series using RFGHG, TRF* and TRF.

where $DT_t^* = t - T_B$ if $t > T_B$ and zero otherwise, T_B denotes the time of the break, t is a time trend, β_2 is the change in slope and $\tilde{y}_t$ is the noise component. Minimizing the sum of squared residuals of regression (1), the break dates for global and Northern Hemisphere from the HadCRUT4 data set are estimated to occur in 1956 and 1966 but for Southern Hemisphere there is evidence of two breaks, in 1909 and 1976, the second being much larger. The NASA data set leads to similar estimates: 1956 for global, 1968 for Northern Hemisphere and for Southern Hemisphere in 1923 and 1955. Hence, all series show clear evidence of a break associated with a large increase in their growth rate around 1960 (Supplementary Information 2.4).

The data-generating processes can be investigated using unit root tests that allow for a one-time break in the trend function. The Kim–Perron test[5,6] provides strong evidence that all temperature series are trend-stationary processes accounting for the documented break, in accordance with results reported for observed and simulated temperatures[3,14] and those in the Supplementary Information 2, except that once the AMO is filtered the estimates of the break dates are not statistically different[15]. An exception is Southern Hemisphere from HadCRUT4 for which the estimate of the break date is 1976. As discussed in the Supplementary Information 1, the difference between Southern Hemisphere from the HadCRUT3 and HadCRUT4 seems to be characterized by an AMO-like low-frequency oscillation. Interestingly, if the effect of AMO is filtered, the estimate of the break date for Southern Hemisphere from HadCRUT4 is 1955 as for Southern Hemisphere from NASA and HadCRUT3. In what follows, we shall continue using 1976 as the break date given that the results are robust to using 1955 or 1976.

All series show a slight warming until the mid-twentieth century: for the HadCRUT4 data, the increase is 0.30 °C, 0.35 °C and 0.27 °C per century for global, Northern Hemisphere and Southern Hemisphere, respectively; for NASA the corresponding figures are 0.31 °C, 0.39 °C and 0.27 °C. At the estimated break dates, the warming rates roughly tripled, with increases of 0.97 °C, 1.18 °C and 1.09 °C per century for HadCRUT4 global, Northern Hemisphere and Southern Hemisphere, and corresponding increases of 0.94 °C, 1.16 °C and 0.93 °C for NASA. The estimates of the post-break warming rates are roughly 1 °C per century for global, Northern Hemisphere and Southern Hemisphere for both data sets. After the break dates the warming has been uniform across hemispheres, as expected from an increase in radiative forcing of well-mixed greenhouse gases[16] once part of the thermal inertia and feedback effects that lead to strong warming differences between land and ocean have been removed by filtering the effects of AMO (Supplementary Information 1). Therefore, the large differences between the estimates of the warming rates and break dates reported using the unfiltered series are caused by the low-frequency natural variability mostly associated with AMO (refs 3,13,14).

Common trends in temperatures and radiative forcing

We provide statistical evidence that the same features are present in the forcing variables, depicted in Fig. 2. They also clearly show a nonstationary behaviour with varying growth rates though, as expected, with much less short-term variability[17]. Applying the same methodologies, the results indicate that all series are trend-stationary processes with a highly significant break in growth rate estimated to occur in 1960 for RFGHG, TRF* and TRF. This date is not statistically different from those of the slope breaks in the filtered temperature series (see Supplementary Table 10 for the confidence intervals). Hence, the temperature and forcing series have stationary noise components around trend functions with nearly common significant breaks in trend slope, indicating a secular co-movement.

To formally test for a common nonlinear trend in temperatures and radiative forcing, a nonparametric nonlinear co-trending test[9] was applied to two sets composed of the global, Northern Hemisphere and Southern Hemisphere temperature series from each data set, RFGHG and TRF. In both cases the results indicate the existence of four co-trending vectors involving global, Northern Hemisphere, Southern Hemisphere, RFGHG and TRF, hence a single common nonlinear trend. This suggests a dominant anthropogenic influence on observed warming. The simplest

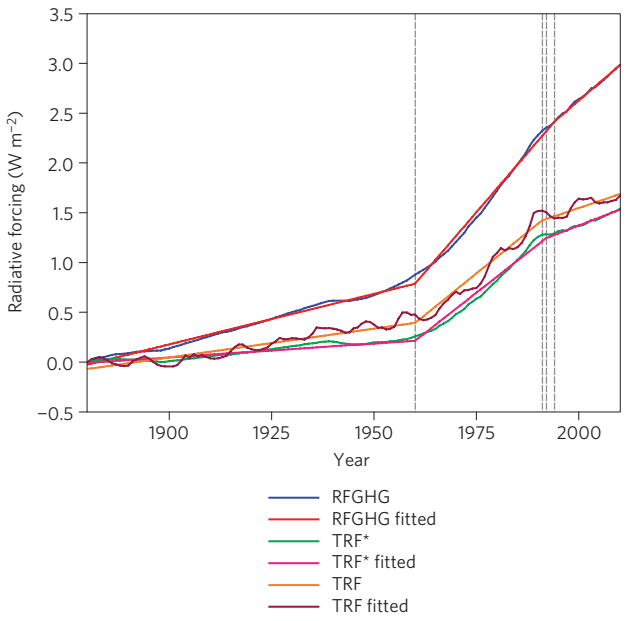

Figure 2 | Aggregated radiative forcing series. Time series plot of RFGHG, TRF* and TRF and the fitted trend functions with two breaks: 1960 and 1994 for RFGHG, 1960 and 1992 for TRF*, 1960 and 1991 for TRF.

radiative forcing series considered in each group is RFGHG, which contains the nonlinear trend present in all other series, indicating it is the dominant driver imparting the common nonlinear trend to TRF and in turn to global, Northern Hemisphere and Southern Hemisphere (Supplementary Table 11).

Figure 1 shows the fitted temperature series obtained from ordinary least squares regression with different forcing series as the explanatory variable and with the filtered global and Northern Hemisphere, and the unfiltered Southern Hemisphere, as the dependent variables. The concordance between the forcing and temperature trends is apparent; in all cases the fitted values seem to be the product of a low-pass filter on temperatures. Visual inspection of the residuals in Supplementary Figs 6a–d strongly suggests that in all cases all secular movements have cancelled, leaving only stationary variations around zero.

The origin of the common trend can be established using the same testing procedure applied to the radiative forcing variables. The results show that the main secular movement of TRF* and TRF is imparted by RFGHG, indicating that human-induced factors are the main drivers behind the observed warming.

The structural model behind this statistical model can be described by means of a simple two-compartment climate model[18,19], for which the temperature in the atmosphere and the upper ocean closely follows the movements of external forcing, owing to small heat capacity and short time constant for reaching its steady state. The slope coefficient relating these two variables is the transient climate sensitivity estimated to be $0.35\,^{\circ}\mathrm{C}(\mathrm{W\,m^{-2}})^{-1}$ and $0.40\,^{\circ}\mathrm{C}(\mathrm{W\,m^{-2}})^{-1}$ for NASA and HadCRUT4, respectively, concordant with previously reported values[18] (see Methods and Supplementary Information 6).

Our results have implications for previous work questioning the relevance of anthropogenic factors to explain the observed warming[20]. Their main conclusion is that previous cointegration-based studies[2,21,22] have overlooked the differences in the order of integration, arguing that radiative forcings are integrated of order two whereas temperatures are integrated of order one. Given our findings, these conflicting results can easily be explained. If, as we claim, both series are trend-stationary with a change in slope, the application of standard unit root tests that misspecify the trend as linear will lead to their spurious results given the magnitude of the noise for each series[5,23] (see Supplementary Information 4, which also includes comparisons with other studies).

Anthropogenic influence on the slow-downs in warming

A relevant implication of our results is that deviations from the secular movement of temperatures are transitory: temperatures are reverting to the underlying trend determined by anthropogenic activities. Therefore, analysing the radiative forcing trend provides a way to investigate smaller variations in the rate of warming that are obscured by the large natural temperature variability relative to the warming signal. The 1940–1970 cooling period and the recent slow-down in warming are of special interest.

Although describing temperature and forcing variables as having piecewise linear trends is convenient to investigate their time series properties, it is a large simplification of the more complex secular movement. The analysis so far revealed that the overwhelming feature of the data is a large change in growth rates near 1960, variations are stationary around these broken trends and radiative forcings and temperatures have a common breaking trend; the break need not be abrupt, a smooth transition is possible. This does not preclude other nonlinearities not detected by statistical tests, such as a transition period or other small breaks.

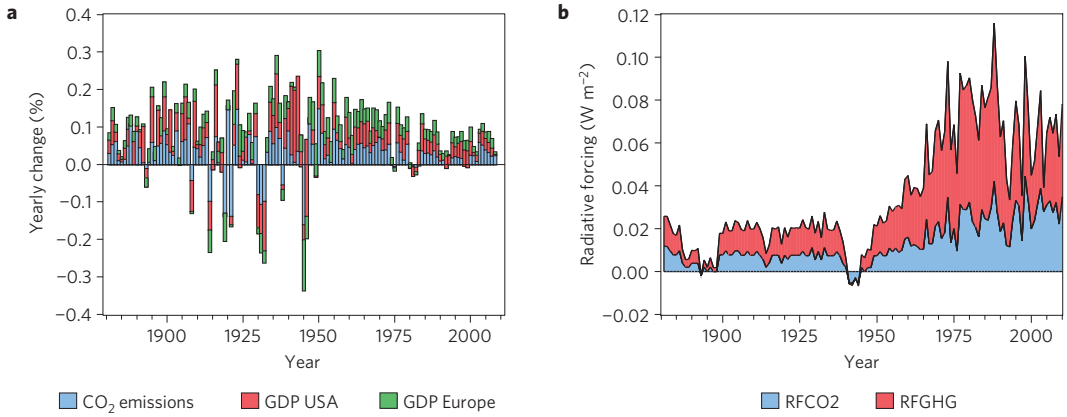

Figure 3 | GDP and CO_2 emissions yearly changes. a, Per cent yearly changes in the GDP of Europe and of the USA, and of the CO_2 global emissions. Dark shaded areas mark World War I and II, and the Great Depression. Light shaded areas represent economic crises that took place within two years of these events. **b**, Yearly changes in the radiative forcing of CO_2 and RFGHG.

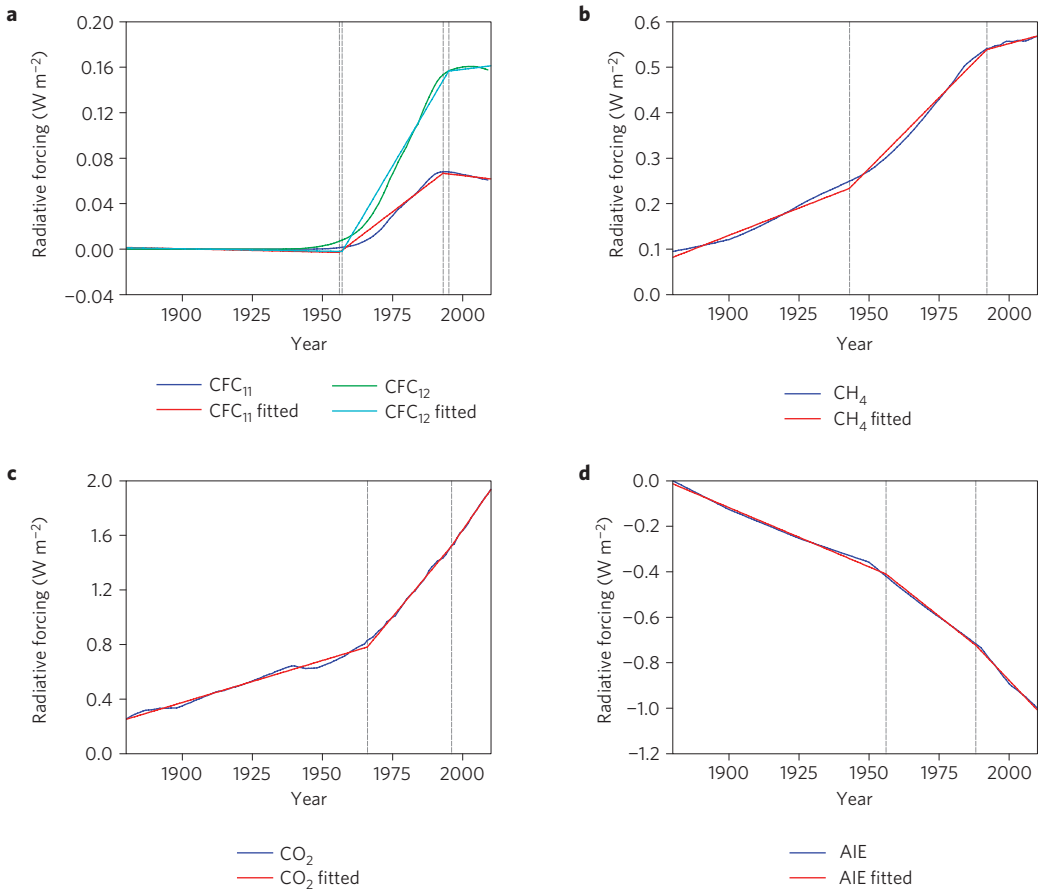

Figure 4 | Trends of CFC_{11}, CFC_{12}, CH_4, CO_2 and AIE. a–d, Time series plot of some components of RFGHG and of AIE along with the fitted trend function with two breaks; the dashed lines indicate the dates of significant breaks: 1956 and 1993 for CFC_{11} (**a**); 1957 and 1995 for CFC_{12} (**a**); 1943 and 1992 for CH_4 (**b**); 1966 and 1996 for CO_2 (**c**); 1956 and 1988 for AIE (**d**).

The cooling period 1940–1970 has been explained as a mixture of natural variability (mainly AMO) and the cooling effect of anthropogenic aerosols (RAER) produced during the industrial recuperation of Europe after World War II (refs 17,24–28). However, even when the effects of AMO are filtered, visual inspection still suggests a slowdown in warming but, notably, with a shorter duration (1938–1955). Also, although the effect of aerosols is mainly limited to Northern Hemisphere, the no-warming period also applies to global and Southern Hemisphere (ref. 26; about −0.07 °C per decade for global, Northern Hemisphere and Southern Hemisphere from HadCRUT4).

Although these factors contributed to the cooling period, the CO_2 radiative forcing (RFCO2) is another cause rarely mentioned. RFGHG from 1938 to the early 1950s experienced a considerable slow-down in growth rate, remaining almost flat during 1938–1947, mainly from a decrease in RFCO2 for almost a decade (1940s, Supplementary Fig. 7b). Otherwise, the cooling effect of RAER would have been mostly compensated by the increase in RFGHG: the yearly rate of growth of RAER during this cooling period was $-0.013\,W\,m^{-2}$ whereas that of RFGHG before the slow-down in RFCO2 was $0.010\,W\,m^{-2}$.

The per cent reduction in CO_2 emissions during 1914–1946 has no parallel since 1751. These reductions were driven by three landmark socioeconomic events occurring in a brief period: the two world wars and the 1929 economic crisis. Figure 3 depicts that during this period negative yearly growth rates were frequent in the gross domestic products (GDPs) of Europe and the USA and in global CO_2 emissions. In particular, the Great Depression of 1929 induced a considerable reduction in world emissions of CO_2 and other greenhouse gases related to economic activity. The largest drop in CO_2 emissions occurred between 1929 and 1932 (26% reduction) recovering its previous level only in 1937 (ref. 29). This led to a four-year period of negative changes in CO_2 and RFGHG (Fig. 3), resulting in an inflection point around 1938 in RFGHG and TRF* (Fig. 2). The post-World-War-II economic expansion and the corresponding sharp and uninterrupted increase in anthropogenic forcing led to the occurrence of the common break in radiative forcing and temperature series around 1960, marking the beginning of sustained global warming.

The causes of a slow-down in warming since the mid-1990s have been a subject of interest. Some proposed the joint effect of increased short-lived sulphur emissions, La Niña events and the eleven-year solar cycle as offsetting the effect of rising greenhouse gas concentrations[22]. We show that the effects of the Montreal Protocol and of changes in agricultural practices in Asia have been large enough to change the long-run path of radiative forcing. Tropospheric aerosols contributed to making this slow-down more pronounced.

The causes of the reduced growth rate of RFGHG are twofold: the reduction of chlorofluorocarbon (CFC) emissions and the pause in the growth rate of atmospheric methane[13,30–32]. The first is a direct consequence of the Montreal Protocol (1989) for controlling substances depleting the stratospheric ozone layer. The second is not completely understood but seems to be related to the decrease in microbial sources caused by the application of chemical fertilizers and to more efficient water use for producing rice in Asia[32].

To obtain statistical evidence about the causes of the smaller increase in temperatures, we search for additional breaks in

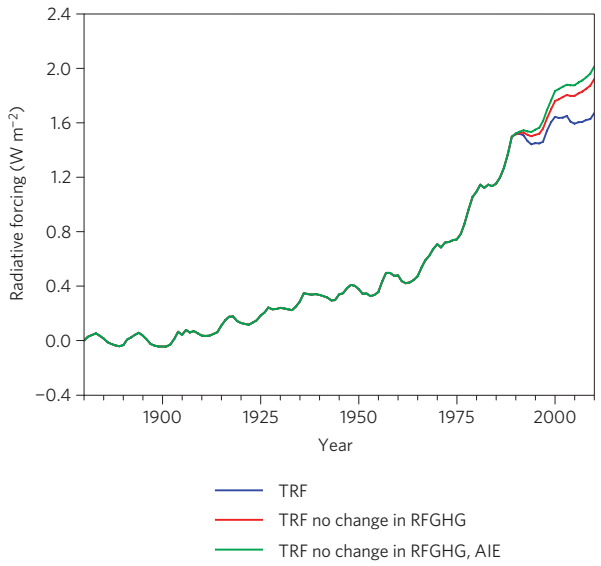

Figure 5 | The effects of the slow-down in RFGHG and the increase in AIE over TRF. Time series plot of TRF, TRF without the break in RFGHG, and TRF without the break in RFGHG and AIE.

the post-1960 period using the sequential Perron–Yabu testing procedure developed by Kejriwal and Perron[7,8]. The slow-down in RFGHG is confirmed by a highly significant reduction of 25.61% in trend slope in 1994. This break is even more pronounced when the direct and indirect effects of tropospheric aerosols are considered, as in TRF* and TRF. The breaks are highly significant, occurred in 1992 and 1991, respectively, and the rates of increase were reduced by more than 50% (the estimated break dates are not statistically different). Figure 2 presents the forcing series with the fitted trends obtained using the two estimated break dates. A similar break is also present in global from NASA: when considering the post-1960 sample, there is a statistically significant break in slope in the mid-1990s consistent with the reported slow-down in warming. This evidence is strong in view of the fact that the sample is quite short, though the result is not robust to using a longer sample. This change in the growth rate of radiative forcing is another common feature of the forcing and temperature trends.

To obtain a better assessment, we applied the sequential break point detection procedure to all components of RFGHG, RAER, the indirect effects of aerosols (AIE) and black carbon. Four components of RFGHG showed a statistically significant break in the post-1990 period (Fig. 4). The largest change occurred for CFC_{11}, with a break in 1993 and 116% decrease in slope, reverting to a sustained decrease. The second in magnitude occurred for CFC_{12} with a break in 1995 and a 92.85% reduction in slope. These results provide clear evidence that the Montreal Protocol was successful in achieving global reductions in CFC emissions. Although not its objective, the reductions were large enough to have an impact on RFGHG, which slowed the increase in warming[31]. The third largest decrease occurred for CH_4, with a break in 1992 and the slope decreasing 73.35%. The last component with a break in the 1990s is CO_2 but it actually exhibits a 19.78% increase in slope in 1996. Hence, the evidence shows that the decrease in CFC_{11} and the reduced increase rate of CFC_{12} and CH_4 are the main contributors to the decrease in the growth rate of TRF, despite the more rapid increase in CO_2. As discussed previously[22,30], another significant factor for the slow-down in warming is the negative effect of the indirect effect of tropospheric aerosols, which shows a 32.48% steeper slope since 1988 (Fig. 4). Without these breaks in the components of the RFGHG, TRF would had been 0.25 W m^{-2} larger in 2010 (about 0.13 W m^{-2}, 0.05 W m^{-2} and 0.08 W m^{-2} for CH_4, CFC_{11} and CFC_{12}, respectively), a small amount compared with the anthropogenic RFGHG but equivalent to a full-amplitude solar cycle forcing[33], and about 15% of the increase in TRF since 1880 (Fig. 5). If, additionally, the break in the indirect effect of tropospheric aerosols is removed, TRF would have been 0.34 W m^{-2} larger, about a fifth of its increase from preindustrial times. Stratospheric aerosols from volcanic eruptions (for example, Mount Pinatubo) cannot be responsible for a long-lasting change as they have a short-lived effect on temperatures (see Supplementary Information 2.1).

Paradoxically the recent decrease in warming, presented by global warming sceptics as proof that humankind cannot affect the climate system, is shown to have a direct human origin.

Methods

Data. The annual temperature data used are from the HadCRUT4 (1850–2010) (http://www.metoffice.gov.uk/hadobs/hadcrut4/data/current/download.html) and the the Goddard Institute for Space Studies (GISS-NASA; 1880–2010) data sets (http://data.giss.nasa.gov/gistemp/). The AMO (1856–2010) was obtained from NOAA (http://www.esrl.noaa.gov/). For the analysis in S1 the following climate indices were used: Southern Oscillation Index (http://www.cgd.ucar.edu/cas/catalog/climind/SOI.signal.ascii); North Atlantic Oscillation (http://climexp.knmi.nl/data/inao.dat); and Pacific Decadal Oscillation (http://jisao.washington.edu/pdo/PDO.latest). For the sensitivity analysis in SI, the HadCRUT3 database was used (http://www.metoffice.gov.uk/hadobs/hadcrut3/).

We also used series from databases related to climate model simulations by GISS-NASA. The radiative forcing data obtained from GISS-NASA (downloaded from http://data.giss.nasa.gov/modelforce/ before the 19 December 2012 revision, data available on request) for the period 1880–2010 include the following (in W m^{-2}): well-mixed greenhouse gases (carbon dioxide, methane, nitrous oxide and CFCs); ozone; stratospheric water vapour; solar irradiance; land-use change; snow albedo; stratospheric aerosols; black carbon; reflective tropospheric aerosols; and the indirect effect of aerosols. The aggregated radiative forcing series were constructed as follows: RFGHG is the radiative forcing of the well-mixed greenhouse gases; TRF* is RFGHG plus the radiative forcing of ozone, stratospheric water vapour, land-use change; snow albedo, black carbon, reflective tropospheric aerosols and the indirect effect of aerosols; TRF is TRF* plus solar irradiance. For the sensitivity analysis in S7, the direct effect of atmospheric aerosols was obtained from the RCP database (http://www.pik-potsdam.de/~mmalte/rcps/index.htm). To analyse the individual components of RFGHG, the global mean mixing ratios of carbon dioxide, methane and CFCs were obtained from GISS-NASA (downloaded from http://data.giss.nasa.gov/modelforce/ghgases// before the 19 December 2012 revision, data available on request); and the radiative forcing owing to these gases was calculated using simplified expressions[34]. The global emissions from fossil fuel burning, cement manufacture and gas flaring are from the Carbon Dioxide Information Analysis Center (http://cdiac.ornl.gov/trends/emis/tre_glob_2008.html). The GDP data (1880–2008) were obtained from the University of Groningen (http://www.ggdc.nl/maddison/).

Structural and time series models. The time series models presented here have the general form:

$$T_t = \alpha + \gamma F_t + \varepsilon_t$$

where T_t is temperature, F_t is some measure of radiative forcing and ε_t is a climate noise encompassing both short-term and longer-term variability modes. The structural model can be described by a simple two-compartment climate model[18,19]. The upper compartment is composed mainly of the atmosphere and the upper ocean and has a small heat capacity and short time constant to reach its steady state. This upper compartment is thermally coupled to the lower compartment, composed of the deep ocean, having a large heat capacity and long time constant for reaching the steady state. When a positive and sustained external forcing is applied to the system, the upper compartment temperature increases, inducing changes in the absorbed and/or emitted radiation at the top of the atmosphere and a heat flow to the lower compartment, which has a much larger heat capacity and requires a much longer time to respond to any forcing. The analyses presented in this paper relate to the response of the upper compartment of the climate system to increases in radiative forcing. The transient climate sensitivity characterized by the short time constant of the upper compartment is:

$$S_{tr} = (\kappa + \lambda)^{-1}$$

where κ is the heat uptake coefficient of the climate system[18]. The transient climate sensitivity relates the time-dependent increase in surface temperature to the time-dependent forcing such that $\Delta T(t) = S_{tr} F(t)$ and it is equal to the

slope parameter γ in the time series model above. The response of the climate system to the forcing over the observed period is determined by the time constant of the upper compartment and the transient climate sensitivity, providing a physical explanation of why global and hemispheric surface temperatures follow the same nonlinear trend of the radiative forcing and why observed temperatures rapidly adjust to changes in the trend of the radiative forcing. These features are particularly clear after part of the low-frequency oscillations produced by AMO are filtered out of both global and Northern Hemisphere. The overlapping confidence intervals in the break dates in the slope functions of radiative forcing and temperature series found here are also consistent with the short time constant dominating this relationship, giving physical support to the idea of co-breaking in surface temperature and radiative forcing series. Supplementary Information 6 also presents a structural interpretation of the trend-stationary nature of aggregate radiative forcing.

Received 28 February 2013; accepted 8 October 2013; published online 10 November 2013

References

1. Hasselmann, K. Multi-pattern fingerprint method for detection and attribution of climate change. *Clim. Dyn.* **13,** 601–611 (1997).
2. Kaufmann, R. K. & Stern, D. I. Evidence for human influence on climate from hemispheric temperature relations. *Nature* **388,** 39–44 (1997).
3. Gay, C., Estrada, F. & Sánchez, A. Global and hemispheric temperature revisited. *Clim. Change* **94,** 333–349 (2009).
4. Estrada, F., Gay, C. & Sánchez, A. A reply to 'Does temperature contain a stochastic trend? Evaluating conflicting statistical results'. *Clim. Change* **101,** 407–414 (2010).
5. Perron, P. The great crash, the oil price shock, and the unit root hypothesis. *Econometrica* **57,** 1361–1401 (1989).
6. Kim, D. & Perron, P. Unit root tests allowing for a break in the trend function under both the null and the alternative hypotheses. *J. Econom.* **148,** 1–13 (2009).
7. Perron, P. & Yabu, T. Testing for shifts in trend with an integrated or stationary noise component. *JBES* **27,** 369–396 (2009).
8. Kejriwal, M. & Perron, P. A sequential procedure to determine the number of breaks in trend with an integrated or stationary noise component. *J. Time Ser. Anal.* **31,** 305–328 (2010).
9. Bierens, H. J. Nonparametric nonlinear cotrending analysis, with an application to interest and inflation in the United States. *JBES* **18,** 323–337 (2000).
10. Wu, Z., Huang, N. E., Wallace, J. M., Smoliak, B. V. & Chen, X. On the time-varying trend in global-mean surface temperature. *Clim. Dyn.* **37,** 759–773 (2011).
11. Swanson, K. L., Sugihara, G. & Tsonis, A. A. Long-term natural variability and the twentieth century climate change. *Proc. Natl Acad. Sci. USA* **106,** 16120–16123 (2009).
12. Knudsen, M. F., Seidenkrantz, M. S., Jacobsen, B. H. & Kuijpers, A. Tracking the Atlantic Multidecadal Oscillation through the last 8,000 years. *Nature Comm.* **2,** 178 (2011).
13. IPCC *Climate Change 2007: The Physical Science Basis*. Solomon, S. et al. (eds), 996 (Cambridge Univ. Press, 2007).
14. Estrada, F., Perron, P., Gay, C. & Martínez, B. A time series analysis of the twentieth century climate simulations produced for the IPCC's AR4. *PLoS ONE* **8,** e60017 (2013).
15. Perron, P. & Zhu, X. Structural breaks with deterministic and stochastic trends. *J. Econom.* **129,** 65–119 (2005).
16. Meehl, G. A., Washington, W. M., Wigley, T. M. L., Arblaster, J. M. & Dai, A. Solar and greenhouse gas forcing and climate response in the twentieth century. *J. Clim.* **16,** 426–444 (2003).
17. Hansen, J. & Sato, M. Greenhouse gas growth rates. *Proc. Natl Acad. Sci. USA* **101,** 16109–16114 (2004).
18. Schwartz, S. E. Determination of Earth's transient and equilibrium climate sensitivities from observations over the twentieth century: strong dependence on assumed forcing. *Surv. Geophys.* **33,** 745–777 (2012).
19. Gregory, J. M. & Forster, P. M. Transient climate response estimated from radiative forcing and observed temperature change. *J. Geophys. Res.* **113,** D23105 (2008).
20. Beenstock, M., Reingewertz, Y. & Paldor, N.. Polynomial cointegration tests of anthropogenic impact on global warming. *ESD* **3,** 173–188 (2012).
21. Kaufmann, R.K., Kauppi, H. & Stock, J. H. Emissions, concentrations, & temperature: a time series analysis. *Clim. Change* **77,** 249–278 (2009).
22. Kaufmann, R. K., Kauppi, H., Mann, M. L. & Stock, J. H. Reconciling anthropogenic climate change with observed temperature 1998–2008. *Proc. Natl Acad. Sci. USA* **108,** 11790–11793 (2011).
23. Perron, P. Testing for a unit root in a time series with a changing mean. *JBES* **8,** 153–162 (1990).
24. Hansen, J. & Lebedeff, S. Global trends of measured surface air temperature. *J. Geophys. Res.* **92,** 13345–13372 (1987).
25. Jones, P. D., Raper, S. C. B., Bradley, R. S., Diaz, H. F., Kelly, P. M. & Wigley, T. M. L. Northern Hemisphere surface air temperature variations: 1851–1984. *J. Clim. App. Meteorol.* **25,** 161–179 (1986).
26. Jones, P. D., Raper, S. C. B. & Wigley, T. M. L. Southern Hemisphere surface air temperature variations: 1851–1984. *J. Clim. App. Meteorol.* **25,** 1213–1230 (1986).
27. Jones, P. D., Wigley, T. M. L. & Wright, P. B. Global temperature variations between 1861 and 1984. *Nature* **322,** 430–434 (1986).
28. Thompson, D. W. J., Kennedy, J. J., Wallace, J. M. & Jones, P. D. A large discontinuity in the mid-twentieth century in observed global mean surface temperature. *Nature* **453,** 646–649 (2008).
29. Andres, R. J., Fielding, D. J., Marland, G., Boden, T. A. & Kumar, N. Carbon dioxide emissions from fossil-fuel use, 1751–1950. *Tellus* **51B,** 759–765 (1999).
30. Hansen, J.E. & Sato, M. Trends of measured climate forcing agents. *Proc. Natl Acad. Sci. USA* **98,** 14778–14783 (2001).
31. Velders, G. J. M. *et al.* The importance of the Montreal Protocol in protecting climate. *Proc. Natl Acad. Sci. USA* **104,** 4814–19 (2007).
32. Kai, F. U., Tyler, S. C., Randerson, J. T. & Blake, D. R. Reduced methane growth rate explained by decreased Northern Hemisphere microbial sources. *Nature* **476,** 194–197 (2011).
33. Hansen, J., Sato, M., Kharecha, P. & von Schuckmann, K. Earth's energy imbalance and implications. *Atmos. Chem. Phys.* **11,** 27031–27105 (2011).
34. Hansen, J., Sato, M., Lacis, A., Ruedy, R., Tegen, I. & Matthews, E. Perspective: Climate forcings in the industrial era. *Proc. Natl Acad. Sci. USA* **95,** 12753–12758 (1998).

Acknowledgements

F.E. acknowledges financial support from the Consejo Nacional de Ciencia y Tecnología (http://www.conacyt.gob.mx) under grant CONACYT-310026, as well as from PASPA DGAPA of the Universidad Nacional Autónoma de México.

Author contributions

F.E. and P.P. contributed equally to the conceptual design, the data analysis and the writing of this manuscript. B.M.L. contributed to the conceptual design and data analysis.

Additional information

Supplementary information is available in the online version of the paper. Reprints and permissions information is available online at www.nature.com/reprints. Correspondence and requests for materials should be addressed to F.E.

Competing financial interests

The authors declare no competing financial interests.